Nano Research 2016, 9(9): 2672–2680
DOI 10.1007/s12274-016-1154-2
Research Article
ISSN 1998-0124
CN 11-5974/O4

Hydrothermal synthesis of manganese oxide encapsulated multiporous carbon nanofibers for supercapacitors

Haiyan Wang, Jiang Deng, Yiqing Chen, Fan Xu, Zhongzhe Wei, and Yong Wang (✉)

Advanced Materials and Catalysis Group, ZJU-NHU United R&D Center, Center for Chemistry of High-Performance and Novel Materials, Department of Chemistry, Zhejiang University, Hangzhou 310028, China

Received: 11 April 2016
Revised: 15 May 2016
Accepted: 16 May 2016

© Tsinghua University Press and Springer-Verlag Berlin Heidelberg 2016

KEYWORDS
hydrothermal carbonization,
multiporous carbon nanofiber,
manganese oxide,
encapsulated,
supercapacitor

ABSTRACT

Hydrothermal carbonization (HTC) of biomass to produce one-dimensional carbon materials with hierarchical pores is of significant importance. Here, we fabricate composites of MnO_x-encapsulated multiporous carbon nanofibers (M-MCNFs) from naturally available carbohydrates through a dopamine-assisted HTC/templating process. The introduction of dopamine aids in the formation of the morphology of carbon nanofibers (CNFs) by enhancing the interactions between the hard-templates and carbohydrates. The chosen cryptomelane hard-templates, which are superior to traditional hard-templates, are converted into Mn_3O_4 nanoparticles embedded in multiporous CNFs (MCNFs), eliminating the need for tedious post deposition procedures to introduce redox active sites. Hence, the obtained hybrids with large surface areas, hierarchical pores, and unique structures show great potential in supercapacitors. This economic and sustainable strategy paves a new way for synthesizing MCNFs and metal oxide-encapsulated MCNFs composites from biomass.

1 Introduction

One-dimensional carbon nanomaterials with peculiar physical and chemical properties have become a hot topic owing to their wide range of applications, including as selective adsorbents, field electron sources, catalyst supports, and electrode materials [1–5]. Up to now, a number of synthetic strategies have been developed to prepare carbon nanofibers (CNFs) and carbon nanotubes (CNTs), such as high-voltage arc discharge [1], chemical vapor deposition [6], laser ablation [7], and high-temperature hydrothermal carbonization (HTC) of organic compounds [8]. Compared with the other techniques, achieving functional carbonaceous materials via the recently rediscovered HTC procedure is more energetically favorable and sustainable because renewable carbon sources are used at low temperatures (130–250 °C) in aqueous media [9–14]. For example, a successful template-directed HTC method was reported to prepare CNFs that

Address correspondence to chemwy@zju.edu.cn

showed potential for various applications [2, 15–17]. However, HTC materials are commonly nonporous and possess unfavorably low surface areas. Moreover, the carbon structures derived after pyrolysis are microporous materials, which suffer from slow mass transport and poor pore accessibility [14, 15, 18–20]. Hence, the development of a new HTC method to prepare CNFs with multiporosity and high surface area is challenging, but of great importance, in particular for pore-related applications such as supercapacitors, as macropores can serve as buffering reservoirs to minimize diffusion distances, while mesopores can enhance electrolyte diffusion, and micropores can continuously increase charge accommodation [21, 22]. Considering the high energy density of pseudocapacitors and the long cycle life and high power density of electric double-layer capacitors, the synthesis of CNFs with both hierarchical pores and a metal oxide encapsulation structure is highly desirable for practical applications in supercapacitors.

Here, we report a new dopamine-assisted HTC/templating route to prepare manganese oxide-encapsulated multiporous CNFs (M-MCNFs, S_{BET} up to 701 $m^2 \cdot g^{-1}$) from inexpensive and renewable glucose. Cryptomelane nanowires and F127 are added to control the formation of CNFs and induce hierarchical pores through hard- and soft-templating processes. Notably, elucidation of the mechanism showed that the introduction of dopamine is crucial to the formation of the morphology. As dopamine is rich in amine and catechol functional groups, it can enhance the interactions between the hard-templates and biomass resources [23]. Moreover, traditional hard-templates require post deposition treatment with several corrosive and toxic reagents (e.g., HF, NH_4HF, or H_2O_2), which is tedious, costly, and environmentally harmful [17, 24, 25]. Superior to these templates, cryptomelane nanowires serve as hard-templates and are subsequently converted into Mn_3O_4 nanoparticles embedded in MCNFs as active redox sites. Hence, M-MCNFs with unique properties, such as a high surface area, hierarchical pores, combined electric double-layer capacitance and pseudocapacitance, and a metal oxide encapsulation structure, are excellent candidates for energy storage applications. In addition, the structural advantages of the as-prepared hybrids lead to excellent rate performance and cycling stability as supercapacitors.

2 Experimental

2.1 Preparation of cryptomelane-type manganese oxide nanowires

Cryptomelane-type manganese oxide nanowires (Fig. S1 in the Electronic Supplementary Material (ESM)) were synthesized by a modified hydrothermal method according to a previous report [26]. Potassium persulfate ($K_2S_2O_8$, 12.2 mmol), potassium sulfate (K_2SO_4, 12.2 mmol), and manganese sulfate monohydrate ($MnSO_4 \cdot H_2O$, 6.1 mmol) were dispersed in 40 mL of H_2O. The mixture was transferred to a Teflon vessel and heated at 250 ℃ for 4 days. The products were washed several times and finally dried at 70 ℃. X-ray diffraction (XRD) experiments showed that the XRD pattern of the nanowires corresponds to cryptomelane-type manganese oxide with the chemical formula of $K_{2-x}Mn_8O_{16}$ (Fig. S2 in the ESM).

2.2 Hydrothermal synthesis of carbon nanomaterials

In a typical synthesis, 0.14 g of as-produced cryptomelane nanowires and 10 mg of dopamine were dispersed in 40 of mL H_2O with vigorous magnetic stirring to obtain a uniform solution. Then, 1.5 g of glucose and 0.2 g of F127 were added into the solution, and the final solution was transferred to a Teflon vessel and maintained at 160 ℃ for 12 h. The HTC products were collected, washed, and dried at 70 ℃. As a result, manganese oxide/hydrothermal multiporous carbonaceous nanofibers (M-HMCNFs) were fabricated. Finally, the products after HTC were annealed under a N_2 atmosphere at 400 ℃ for 1 h and then heated to 800 ℃ to obtain M-MCNFs. The amount of carbon in M-MCNFs was estimated to be about 81 wt.% using thermogravimetric analysis (TGA) (Fig. S3 in the ESM). Similarly, for comparison, manganese oxide/hydrothermal carbonaceous nanofibers (M-HCNFs) were synthesized by the same method without the addition of F127. The products obtained after HTC were annealed under a N_2 atmosphere at 800 ℃ to obtain M-CNFs. Meanwhile, MCNFs were fabricated

by removing Mn_3O_4 from M-MCNFs with 2 M HCl. To show the important role of dopamine in formation of the morphology, 0.14 g of cryptomelane nanowires and 1.5 g of glucose were dispersed in 40 mL of H_2O. Then, the solution was transferred to a Teflon vessel and maintained at 160 ℃ for 12 h, and the products were collected, washed, and dried at 70 ℃.

2.3 Characterization

Scanning electron microscopy (SEM) images were obtained using a Hitachi SU-8010 microscope. Transmission electron microscopy (TEM) analysis was carried out using a Hitachi HT-7700 microscope. High-resolution transmission electron microscopy (HRTEM) and energy-dispersive X-ray spectrum (EDS) mapping were carried out using a Tecnai G2 F30 S-Twin microscope at an acceleration voltage of 300 kV. X-ray diffraction (XRD) data was collected with a D/tex-Ultima TV wide angle X-ray diffractometer equipped with Cu Kα radiation (λ = 1.54 Å). Raman scattering spectra were collected on a Raman spectrometer (JY, HR 800) using a 514 nm laser. X-ray photoelectron spectra (XPS) were obtained using an ESCALAB MARK II spherical analyzer with an aluminum anode (1,486.6 eV) X-ray source.

2.4 Electrochemical measurements

Electrochemical measurements were performed using three-electrode and two-electrode test systems. The electrochemical performance was based on the total weight of materials on the electrode. To prepare the working electrodes, 90 wt.% of as-obtained products was mixed with 10 wt.% of polytetrafluoroethylene (PTFE) in 1 mL of ethanol to form a homogeneous paste. Then, 500 μL of the mixture was dropped onto nickel foam (1 cm^2) and dried. The mass loading of materials on the working electrodes was about 2–3 mg. Before the electrochemical tests, the foam with the sample was compressed. A platinum sheet and a saturated calomel electrode were used as the counter and reference electrodes, respectively, for three-electrode tests. For the two- electrode test system, two working electrodes were prepared in the same way of that in three-electrode test system. Then these two electrodes were placed face to face with a filter paper separator and finally assembled in a bag filled with electrolytes. The electrochemical measurements were performed on a LAND CT2001A workstation and a Gamry Reference 600 electrochemical workstation.

3 Results and discussion

M-CNFs and M-MCNFs were synthesized using dopamine-assisted HTC/templating. Specifically, a mixture of glucose, dopamine, and cryptomelane-type manganese oxide nanowires underwent a HTC procedure at 160 ℃, with or without F127 as an additive. Then the resultant products were calcined at 800 ℃ (Fig. S4 in the ESM). The SEM images of both M-CNFs and M-MCNFs show nanofibers interwoven together, and no carbon spheres are observed (Figs. 1(a) and 1(b)). However, a large amount of carbonaceous spheres is produced in the absence of dopamine (Fig. S5 in the ESM), indicating that dopamine is critical for the formation of nanofibers. The detailed structural differences between M-MCNFs and M-CNFs were observed using TEM. Unlike M-CNFs (Fig. 1(c)), mesopores exist in M-MCNFs owing to the addition of F127 (Fig. 1(d)). Moreover, as shown in Fig. 1(e), manganese oxide nanoparticles with sizes of 15–27 nm are embedded in the MCNFs with relative uniformity. These nanoparticles are crystalline and correspond to Mn_3O_4, as confirmed by HRTEM (Fig. 1(f)) [27].

The XPS spectrum of M-MCNFs further confirmed the coexistence of C, O, and Mn elements (Fig. 2(a)). In the Mn 2p spectrum (Fig. 2(b)), two strong peaks are observed centered at 653.3 and 641.4 eV, with a splitting of the Mn 2p doublet of 11.9 eV, corresponding to Mn_3O_4 [28]. Figure 2(c) shows the XRD pattern of M-MCNFs. Several relatively intense peaks at 32°, 36°, 38°, and 60° can be assigned to Mn_3O_4 [27, 28], and the sharp peaks at 25° and 44° can be indexed to the (002) and (100) planes, respectively, of graphite. Moreover, a characteristic peak in the Raman spectrum at 650 cm^{-1} can be assigned to Mn_3O_4 (Fig. 2(d)) [28]. In general, the results obtained demonstrated the existence of Mn_3O_4. Furthermore, the N_2 adsorption–desorption isotherm and pore size distribution (Fig. S6 in the ESM) also indicate the existence of a pore structure containing micro- and mesopores in M-MCNFs, which is in accordance with the TEM and

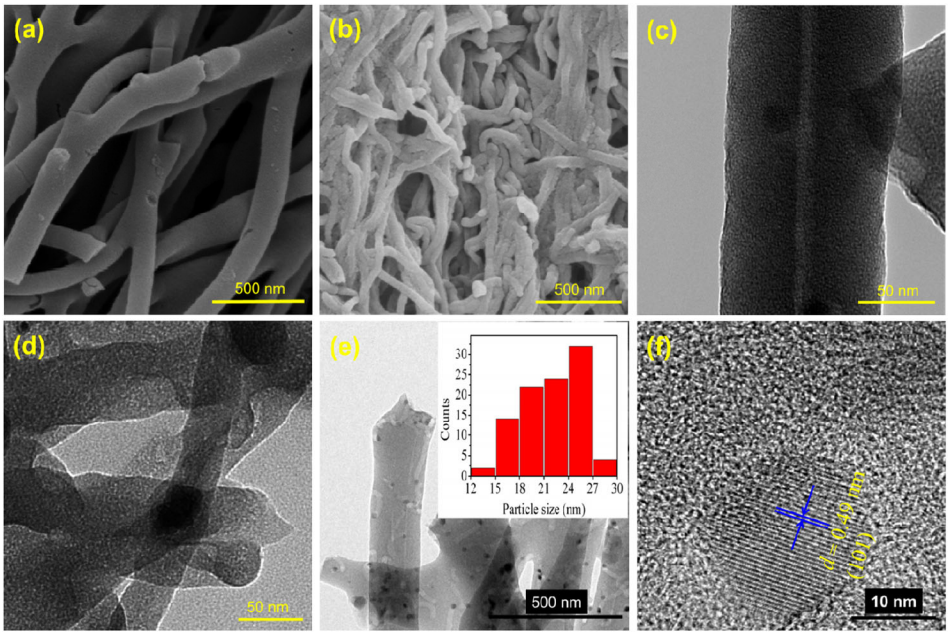

Figure 1 Morphology and microstructures of M-CNFs and M-MCNFs. SEM images of (a) M-CNFs and (b) M-MCNFs. TEM images of (c) M-CNFs and (d) M-MCNFs. (e) and (f) HRTEM images and particle size distribution of M-MCNFs.

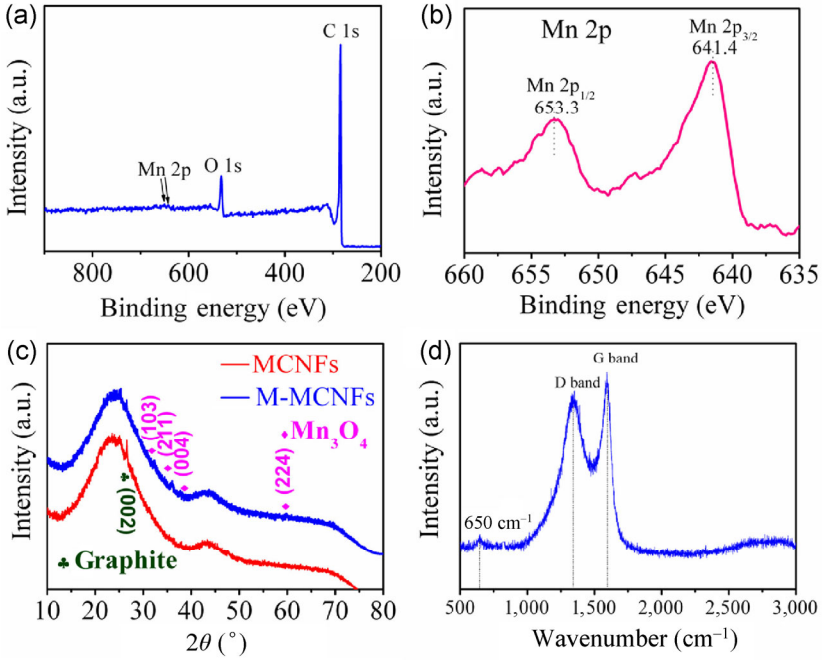

Figure2 Spectroscopic analyses of M-MCNFs. (a) XPS survey spectra. (b) High-resolution Mn 2p XPS spectrum. (c) XRD patterns of M-MCNFs (blue) and MCNFs (red). (d) Raman spectrum of M-MCNFs.

SEM results. The specific surface area (SSA) and volume of mesopores for M-MCNFs (701 $m^2 \cdot g^{-1}$ and 0.58 $cm^3 \cdot g^{-1}$, respectively) were larger than those for M-CNFs (420 $m^2 \cdot g^{-1}$ and 0.1 $cm^3 \cdot g^{-1}$, respectively) suggesting that the presence of F127 during the HTC process induced the formation of mesopores.

To determine the formation mechanism during the HTC procedure, confirmatory experiments were conducted to prove the crucial role of dopamine for formation of carbonaceous nanofiber structures. SEM

and TEM images (Figs. S7(a) and S7(b) in the ESM) show that the HTC products of a mixture containing glucose, dopamine, and cryptomelane nanowires are composed of interlinked fibers with diameters of around 100 nm. If the same experiment is conducted in the absence of glucose, the diameter and length of the nanowires does not change significantly after hydrothermal treatment (Fig. S8(a) in the ESM). However, in the absence of dopamine, no nanowires are formed, but many carbonaceous spheres are observed (Fig. S8(b) in the ESM). This result indicates that dopamine, which is rich in amine and catechol functional groups, acts as a cross-linker and contributes to the adsorption and polymerization of glucose molecules on the hard-templates. Moreover, the cryptomelane nanowires are converted into small particles embedded in carbon (Fig. S8(b) in the ESM) owing to corrosion under acidic condition and hydrothermal reduction of high valence manganese with glucose. A proposed formation mechanism for CNFs with a Mn_3O_4-encapsulated structure is shown in Fig. 3. Dopamine precursors adhere to and polymerize on the surface of the nanowires during the early stage of the stirring process, which introduces functional groups such as –OH and $–NH_2$ on the nanowire surfaces. Then, glucose molecules, which are rich in –OH groups, are deposited on the surface of the functionalized nanowires via adsorption, dehydration, and polymerization. Further, through dehydration, the glucose precursors are gradually transformed into 5-hydroxymethylfurfural (5-HMF) at 160 °C [29]. With time, more glucose molecules around the templates are transformed *in situ* into carbonaceous nanofibers through continuous adsorption, dehydration, polymerization, and crosslinking processes. As a result, HTC CNFs are formed. After hydrothermal treatment, the solution is acidic (pH = 3) and contains some manganese ions. These findings demonstrate that the cryptomelane nanowires are gradually corroded in acidic conditions. Meanwhile, high valence manganese can react with the hydrolyzate of glucose through a hydrothermal reduction route. Therefore, the nanowires are gradually shortened, turning into small rods or manganese ions. After calcination at an elevated temperature, the MnO_x rods are converted into Mn_3O_4 nanoparticles, leaving a hollow structure with mesopores

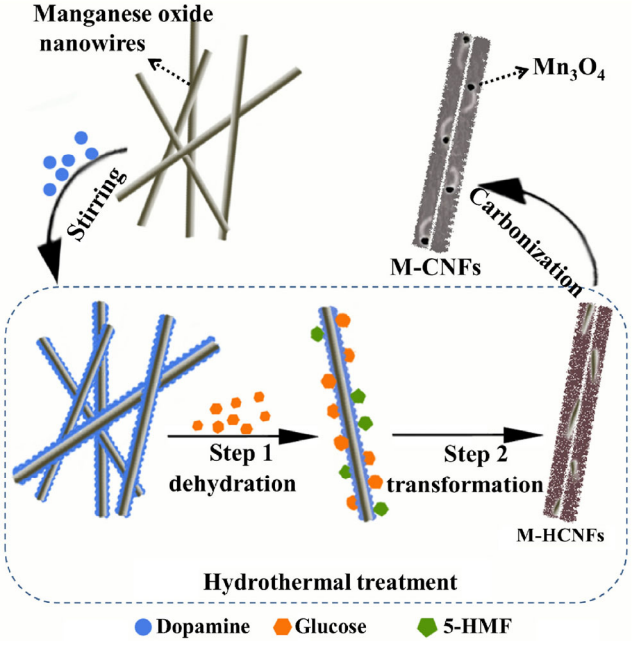

Figure 3 Illustration of the mechanism for formation of M-CNFs.

(Figs. S7(d)–S7(f) in the ESM). Thus, M-CNFs are produced through this dopamine-assisted HTC route.

Because of their larger SSA and hierarchical pore structure including macropores, mesopores, and micropores, M-MCNFs are superior to M-CNFs for energy storage. Galvanostatic charge/discharge (GCD) and cyclic voltammetry (CV) tests of M-MCNFs were performed in 6 M KOH electrolytes, with test of MCNFs (Mn_3O_4 removed) and M-CNFs as comparisons. As shown in Figs. 4(a) and. 4(b), M-MCNFs exhibit the largest CV loop with a significantly prolonged discharge time, indicating that Mn_3O_4 and hierarchical pores are important for enhancing the capacitive performance of M-MCNFs. Mn_3O_4 in M-MCNFs contributes to 55% of the capacitance, as the discharge time of M-MCNFs is 79% longer than that of MCNFs (Fig. 4(b)), and the carbon content is 81%, as measured by TGA (Fig. S3 in the ESM). An evident cathodic peak in the negative scan is observed in the CV curve of M-MCNFs owing to faradaic redox reactions. This result suggests that the multipores in M-MCNFs facilitate contact between ions and active redox sites. In addition, electrochemical impedance spectroscopy (EIS) analysis (Fig. 4(c)) shows that M-MCNFs have a smaller semicircle and lower equivalent series resistance (ESR) of 0.20 Ω than M-CNFs (0.47 Ω), indicating faster electron and ion transport. Therefore,

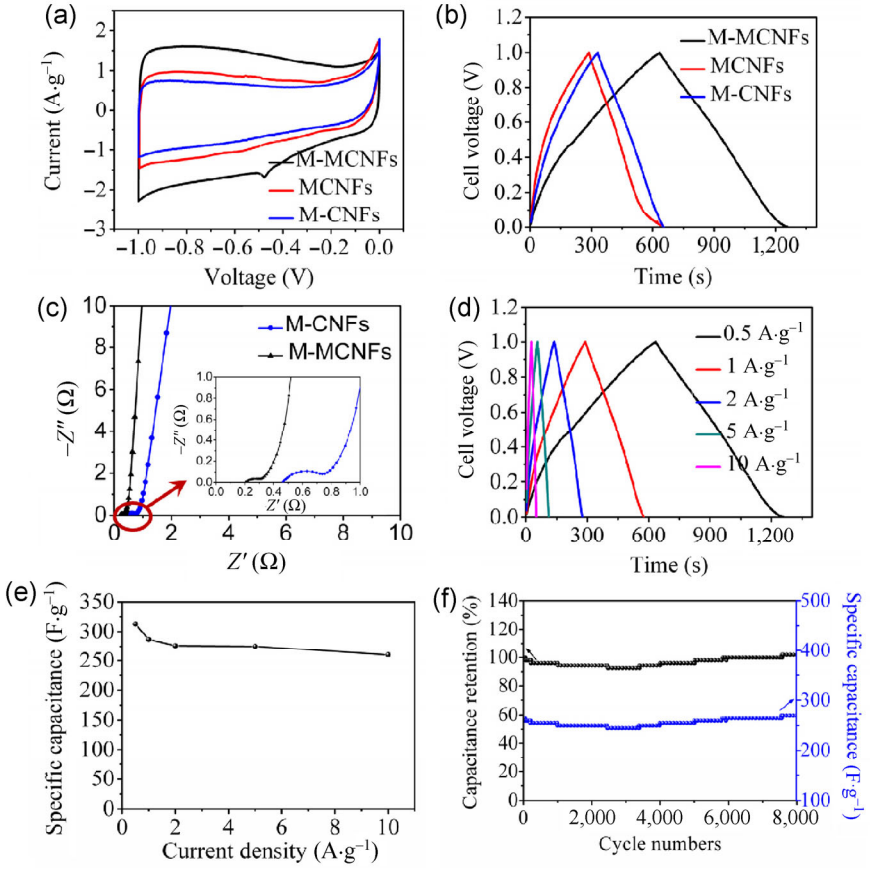

Figure 4 Electrochemical performance of the hybrids measured using a three-electrode system in 6 M KOH solution. (a) CV curves of M-MCNFs, MCNFs, and M-CNFs at a scan rate of 5 mV·s^{-1}. (b) GCD tests of M-MCNFs, MCNFs, and M-CNFs at a current density of 0.5 A·g^{-1}. (c) Nyquist plots for M-MCNFs (black) and M-CNFs (blue) based supercapacitors. (d) Charge–discharge curves of a M-MCNFs electrode at various current densities. (e) Specific capacitance of an M-MCNFs electrode at different current densities. (f) Capacitance retention (black) and specific capacitance (blue) of a M-MCNFs based supercapacitor device measured at a current density of 5 A·g^{-1} over 8,000 charge–discharge cycles.

an enhanced synergistic pseudocapacitance and electric double-layer capacitance effect has been achieved for M-MCNFs.

More detailed electrochemical information was obtained for M-MCNFs using three- and two-electrode tests. The CV curves (Fig. S9 in the ESM) maintain a quasi-rectangular shape, even at a high rate of 200 mV·s^{-1}, indicating desirable fast charge/discharge properties. As shown in Figs. 4(d) and 4(e), M-MCNFs yield a high specific capacitance of 313 F·g^{-1} (645 mF·cm^{-2}) based on the entire mass of the electrode material at a current density of 0.5 A·g^{-1}, which is comparable to that reported for other manganese oxide-based materials, such as MnO_2/graphene/conducting polymer [30], SWCNTs@MnO_2/polypyrrole [31], porous MnO_2 tubular arrays [32], and others [33–36]. In addition, 100% capacitance retention was achieved over 8,000 cycles (Fig. 4(f)), suggesting that hierarchical multiporous carbon not only serves as a conductive wrapping, but also a barrier for Mn_3O_4 nanoparticles, thus enhancing their electrochemical stability. Further, M-MCNFs were assembled and measured in a two-electrode full cell configuration to establish their applicability in practical devices. The specific capacitance of M-MCNFs (Fig. 5(a)) exhibits excellent rate performance, with 88% capacitance retention when the current density increased by a factor of 50. This excellent rate capability can be attributed to the enhanced diffusion of ions resulting from the hierarchical pore structure, high SSA, and good electric conductivity. The performance of M-MCNFs electrodes in aqueous electrochemical cells was further confirmed using

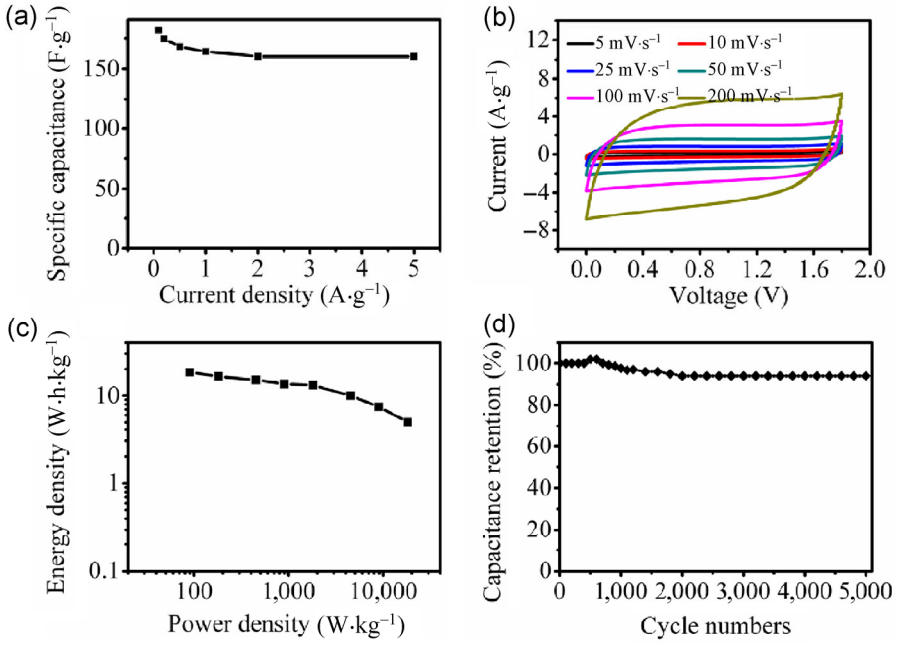

Figure 5 Electrochemical characterization of a M-MCNFs based full cell supercapacitor using a two-electrode test system. (a) Specific capacitance of an M-MCNFs electrode at different current densities in 6 M KOH solution. (b) CV curves of a M-MCNFs based full cell supercapacitor measured in 1 M Na_2SO_4 solution. (c) Ragone plot of a M-MCNFs based full cell supercapacitor measured in 1 M Na_2SO_4 solution. (d) Cycling performance of the full cell capacitor measured in 1 M Na_2SO_4 solution.

another electrolyte, Na_2SO_4, which allows higher operating voltages up to 1.8 V (Fig. 5(b) and Fig. S10 in the ESM). The capacitor in Na_2SO_4 solution shows a highest energy density of 18 W·h·kg^{-1} (Fig. 5(c)) and excellent cyclic stability, with only 6% capacitance loss after 5,000 cycles (Fig. 5(d)). This performance is comparable to that reported for metal oxide-based devices [31, 33, 37–40].

4 Conclusions

In summary, a novel dopamine-assisted HTC/templating method was developed to synthesize M-MCNFs. In the HTC processes, we elucidated that the assembly of glucose with the hard-templates was controlled by the addition of dopamine. The obtained hybrids have a large surface area and a hierarchical pore structure containing macro-, meso-, and micropores. In addition, unlike conventional hard-templates that require tedious post deposition procedures, our chosen cryptomelane nanowire template turned into Mn_3O_4 nanoparticles embedded in the MCNFs, thus providing redox sites. Indeed, the structural advantages of M-MCNFs provide excellent rate performance and cycle stability. Therefore, this economic and sustainable strategy for synthesizing M-MCNFs composites from biomass offers vast opportunities in energy storage applications.

Acknowledgements

Financial support from National Natural Science Foundation of China (Nos. 21376208 and 91534114), the Zhejiang Provincial Natural Science Foundation for Distinguished Young Scholars of China (No. LR13B030001), the Fundamental Research Funds for the Central Universities, and the Partner Group Program of the Zhejiang University and the Max-Planck Society is appreciated greatly.

Electronic Supplementary Material: Supplementary material (detailed experimental procedures, calculation formula, SEM and TEM images, XRD patterns, TGA curves, nitrogen adsorption-desorption isotherms, electrochemical data, and additional references) is available in the online version of this article at http://dx.doi.org/10.1007/s12274-016-1154-2.

References

[1] Iijima, S. Helical microtubules of graphitic carbon. *Nature* **1991**, *354*, 56–58.

[2] Liang, H.-W.; Wang, L.; Chen, P.-Y.; Lin, H.-T.; Chen, L.-F.; He, D.; Yu, S.-H. Carbonaceous nanofiber membranes for selective filtration and separation of nanoparticles. *Adv. Mater.* **2010**, *22*, 4691–4695.

[3] Liang, H.-W.; Cao, X.; Zhang, W.-J.; Lin, H.-T.; Zhou, F.; Chen, L.-F.; Yu, S.-H. Robust and highly efficient free-standing carbonaceous nanofiber membranes for water purification. *Adv. Funct. Mater.* **2011**, *21*, 3851–3858.

[4] Planeix, J. M.; Coustel, N.; Coq, B.; Brotons, V.; Kumbhar, P. S.; Dutartre, R.; Geneste, P.; Bernier, P.; Ajayan, P. M. Application of carbon nanotubes as supports in heterogeneous catalysis. *J. Am. Chem. Soc.* **1994**, *116*, 7935–7936.

[5] Cavaliere, S.; Subianto, S.; Savych, I.; Jones, D. J.; Rozière, J. Electrospinning: Designed architectures for energy conversion and storage devices. *Energy Environ. Sci.* **2011**, *4*, 4761–4785.

[6] Jiang, K. L.; Li, Q. Q.; Fan, S. S. Nanotechnology: Spinning continuous carbon nanotube yarns. *Nature* **2002**, *419*, 801.

[7] Thess, A.; Lee, R.; Nikolaev, P.; Dai, H. J.; Petit, P.; Robert, J.; Xu, C. H.; Lee, Y. H.; Kim, S. G.; Rinzler, A. G. et al. Crystalline ropes of metallic carbon nanotubes. *Science* **1996**, *273*, 483–487.

[8] Jiang, Y.; Wu, Y.; Zhang, S. Y.; Xu, C. Y.; Yu, W. C.; Xie, Y.; Qian, Y. T. A catalytic-assembly solvothermal route to multiwall carbon nanotubes at a moderate temperature. *J. Am. Chem. Soc.* **2000**, *122*, 12383–12384.

[9] White, R. J.; Budarin, V.; Luque, R.; Clark, J. H.; Macquarrie, D. J. Tuneable porous carbonaceous materials from renewable resources. *Chem. Soc. Rev.* **2009**, *38*, 3401–3418.

[10] Zhang, P. F.; Yuan, J. Y.; Fellinger, T.-P.; Antonietti, M.; Li, H. R.; Wang, Y. Improving hydrothermal carbonization by using poly(ionic liquid)s. *Angew. Chem., Int. Ed.* **2013**, *52*, 6028–6032.

[11] White, R. J.; Antonio, C.; Budarin, V. L.; Bergström, E.; Thomas-Oates, J.; Clark, J. H. Polysaccharide-derived carbons for polar analyte separations. *Adv. Funct. Mater.* **2010**, *20*, 1834–1841.

[12] Wang, S. P.; Han, C. L.; Wang, J.; Deng, J.; Zhu, M. L.; Yao, J.; Li, H. R.; Wang, Y. Controlled synthesis of ordered mesoporous carbohydrate-derived carbons with flower-like structure and N-doping by self-transformation. *Chem. Mater.* **2014**, *26*, 6872–6877.

[13] Fang, Y.; Gu, D.; Zou, Y.; Wu, Z. X.; Li, F. Y.; Che, R. C.; Deng, Y. H.; Tu, B.; Zhao, D. Y. A low-concentration hydrothermal synthesis of biocompatible ordered mesoporous carbon nanospheres with tunable and uniform size. *Angew. Chem., Int. Ed.* **2010**, *49*, 7987–7991.

[14] Sevilla, M.; Fuertes, A. B. The production of carbon materials by hydrothermal carbonization of cellulose. *Carbon* **2009**, *47*, 2281–2289.

[15] Hu, B.; Wang, K.; Wu, L. H.; Yu, S.-H.; Antonietti, M.; Titirici, M.-M. Engineering carbon materials from the hydrothermal carbonization process of biomass. *Adv. Mater.* **2010**, *22*, 813–828.

[16] Liang, H.-W.; Liu, J.-W.; Qian, H.-S.; Yu, S.-H. Multiplex templating process in one-dimensional nanoscale: Controllable synthesis, macroscopic assemblies, and applications. *Acc. Chem. Res.* **2013**, *46*, 1450–1461.

[17] Liang, H.-W.; Guan, Q.-F.; Chen, L.-F.; Zhu, Z.; Zhang, W.-J.; Yu, S.-H. Macroscopic-scale template synthesis of robust carbonaceous nanofiber hydrogels and aerogels and their applications. *Angew. Chem., Int. Ed.* **2012**, *51*, 5101–5105.

[18] Ryu, J.; Suh, Y.-W.; Suh, D. J.; Ahn, D. J. Hydrothermal preparation of carbon microspheres from mono-saccharides and phenolic compounds. *Carbon* **2010**, *48*, 1990–1998.

[19] Titirici, M.-M.; Antonietti, M.; Baccile, N. Hydrothermal carbon from biomass: A comparison of the local structure from poly- to monosaccharides and pentoses/hexoses. *Green Chem.* **2008**, *10*, 1204–1212.

[20] Wohlgemuth, S.-A.; White, R. J.; Willinger, M.-G.; Titirici, M.-M.; Antonietti, M. A one-pot hydrothermal synthesis of sulfur and nitrogen doped carbon aerogels with enhanced electrocatalytic activity in the oxygen reduction reaction. *Green Chem.* **2012**, *14*, 1515–1523.

[21] Wang, D.-W.; Li, F.; Liu, M.; Lu, G. Q.; Cheng, H.-M. 3D aperiodic hierarchical porous graphitic carbon material for high-rate electrochemical capacitive energy storage. *Angew. Chem., Int. Ed.* **2008**, *47*, 373–376.

[22] Deng, J.; Xiong, T. Y.; Xu, F.; Li, M. M.; Han, C. L.; Gong, Y. T.; Wang, H. Y.; Wang, Y. Inspired by bread leavening: One-pot synthesis of hierarchically porous carbon for supercapacitors. *Green Chem.* **2015**, *17*, 4053–4060.

[23] Lee, H.; Dellatore, S. M.; Miller, W. M.; Messersmith, P. B. Mussel-inspired surface chemistry for multifunctional coatings. *Science* **2007**, *318*, 426–430.

[24] Mane, G. P.; Talapaneni, S. N.; Anand, C.; Varghese, S.; Iwai, H.; Ji, Q. M.; Ariga, K.; Mori, T.; Vinu, A. Preparation of highly ordered nitrogen-containing mesoporous carbon from a gelatin biomolecule and its excellent sensing of acetic acid. *Adv. Funct. Mater.* **2012**, *22*, 3596–3604.

[25] Lu, A. H.; Kiefer, A.; Schmidt, W.; Schüth, F. Synthesis of polyacrylonitrile-based ordered mesoporous carbon with tunable pore structures. *Chem. Mater.* **2004**, *16*, 100–103.

[26] Yuan, J. K.; Liu, X. G.; Akbulut, O.; Hu, J. Q.; Suib, S. L.; Kong, J.; Stellacci, F. Superwetting nanowire membranes for selective absorption. *Nat. Nanotechnol.* **2008**, *3*, 332–336.

[27] Wang, B.; Park, J.; Wang, C. Y.; Ahn, H.; Wang, G. X. Mn_3O_4 nanoparticles embedded into graphene nanosheets: Preparation, characterization, and electrochemical properties for supercapacitors. *Electrochim. Acta* **2010**, *55*, 6812–6817.

[28] Qu, J. Y.; Gao, F.; Zhou, Q.; Wang, Z. Y.; Hu, H.; Li, B. B.; Wan, W. B.; Wang, X. Z.; Qiu, J. S. Highly atom-economic synthesis of graphene/Mn_3O_4 hybrid composites for electrochemical supercapacitors. *Nanoscale* **2013**, *5*, 2999–3005.

[29] Kimura, H.; Nakahara, M.; Matubayasi, N. *In situ* kinetic study on hydrothermal transformation of D-glucose into 5-hydroxymethylfurfural through d-fructose with ^{13}C NMR. *J. Phys. Chem. A* **2011**, *115*, 14013–14021.

[30] Yu, G. H.; Hu, L. B.; Liu, N.; Wang, H. L.; Vosgueritchian, M.; Yang, Y.; Cui, Y.; Bao, Z. Enhancing the supercapacitor performance of graphene/MnO_2 nanostructured electrodes by conductive wrapping. *Nano Lett.* **2011**, *11*, 4438–4442.

[31] Liang, K.; Gu, T. L.; Cao, Z. Y.; Tang, X. Z.; Hu, W. C.; Wei, B. Q. *In situ* synthesis of SWNTs@MnO_2/polypyrrole hybrid film as binder-free supercapacitor electrode. *Nano Energy* **2014**, *9*, 245–251.

[32] Li, F.; Zhang, Y. X.; Huang, M.; Xing, Y.; Zhang, L. L. Rational design of porous MnO_2 tubular arrays via facile and templated method for high performance supercapacitors. *Electrochim. Acta* **2015**, *154*, 329–337.

[33] Zhao, L.; Yu, J.; Li, W. J.; Wang, S. G.; Dai, C. L.; Wu, J. W.; Bai, X. D.; Zhi, C. Y. Honeycomb porous MnO_2 nanofibers assembled from radially grown nanosheets for aqueous supercapacitors with high working voltage and energy density. *Nano Energy* **2014**, *4*, 39–48.

[34] Yang, P. H.; Ding, Y.; Lin, Z. Y.; Chen, Z. W.; Li, Y. Z.; Qiang, P. F.; Ebrahimi, M.; Mai, W. J.; Wong, C. P.; Wang, Z. L. Low-cost high-performance solid-state asymmetric supercapacitors based on MnO_2 nanowires and Fe_2O_3 nanotubes. *Nano Lett.* **2014**, *14*, 731–736.

[35] Cheng, Y. W.; Lu, S. T.; Zhang, H. B.; Varanasi, C. V.; Liu, J. Synergistic effects from graphene and carbon nanotubes enable flexible and robust electrodes for high-performance supercapacitors. *Nano Lett.* **2012**, *12*, 4206–4211.

[36] Hou, Y.; Cheng, Y. W.; Hobson, T.; Liu, J. Design and synthesis of hierarchical MnO_2 nanospheres/carbon nanotubes/conducting polymer ternary composite for high performance electrochemical electrodes. *Nano Lett.* **2010**, *10*, 2727–2733.

[37] He, Y. M.; Chen, W. J.; Li, X. D.; Zhang, Z. X.; Fu, J. C.; Zhao, C. H.; Xie, E. Q. Freestanding three-dimensional graphene/MnO_2 composite networks as ultralight and flexible supercapacitor electrodes. *ACS Nano* **2013**, *7*, 174–182.

[38] Zhi, J.; Deng, S.; Wang, Y. F.; Hu, A. G. Highly ordered metal oxide nanorods inside mesoporous silica supported carbon nanomembranes: High performance electrode materials for symmetrical supercapacitor devices. *J. Phys. Chem. C* **2015**, *119*, 8530–8536.

[39] Liu, X. J.; Liu, J. F.; Sun, X. M. $NiCo_2O_4$@NiO hybrid arrays with improved electrochemical performance for pseudocapacitors. *J. Mater. Chem. A* **2015**, *3*, 13900–13905.

[40] Wu, M.-S.; Hsu, W.-H. Nickel nanoparticles embedded in partially graphitic porous carbon fabricated by direct carbonization of nickel-organic framework for high-performance supercapacitors. *J. Power Sources* **2015**, *274*, 1055–1062.